Molecular Biology of the Cell
Vol. 10, 4311–4326, December 1999

Receptor-mediated Endocytosis in the *Caenorhabditis elegans* Oocyte

Barth Grant* and David Hirsh

Columbia University College of Physicians and Surgeons, Department of Biochemistry and Molecular Biophysics, New York, New York 10032

Submitted August 13, 1999; Accepted September 24, 1999
Monitoring Editor: Judith Kimble

The *Caenorhabditis elegans* oocyte is a highly amenable system for forward and reverse genetic analysis of receptor-mediated endocytosis. We describe the use of transgenic strains expressing a vitellogenin::green fluorescent protein (YP170::GFP) fusion to monitor yolk endocytosis by the *C. elegans* oocyte in vivo. This YP170::GFP reporter was used to assay the functions of *C. elegans* predicted proteins homologous to vertebrate endocytosis factors using RNA-mediated interference. We show that the basic components and pathways of endocytic trafficking are conserved between *C. elegans* and vertebrates, and that this system can be used to test the endocytic functions of any new gene. We also used the YP170::GFP assay to identify *rme* (receptor-mediated endocytosis) mutants. We describe a new member of the low-density lipoprotein receptor superfamily, RME-2, identified in our screens for endocytosis defective mutants. We show that RME-2 is the *C. elegans* yolk receptor.

INTRODUCTION

Receptor-mediated endocytosis, an essential process in all eukaryotes, is required for general cellular functions, including uptake of nutrients (e.g., low-density lipoprotein [LDL] or transferrin) and recycling of membranes and membrane proteins (Mukherjee *et al.*, 1997). Yolk uptake by growing oocytes is a dramatic example of the receptor-mediated endocytosis pathway in many species, including invertebrates such as the nematode *Caenorhabditis elegans* and vertebrates such as the chicken (Schneider, 1996). *C. elegans* yolk is secreted from its site of synthesis, the intestine, into the pseudoceolomic space (body cavity) and is ultimately taken up into vesicles within the growing oocytes (Kimble and Sharrock, 1983; Hall *et al.*, 1999). Yolk transport in vertebrates such as the chicken follows a similar route, from liver to bloodstream to ovum (Schneider, 1996).

Yolk is a lipoprotein particle composed of lipids and lipid-binding proteins called vitellogenins. Vitellogenins are among the most abundant proteins found in developing embryos (Sharrock, 1983). Lipids and proteins derived from yolk are thought to provide essential nutrients required to support the rapid development of the embryo. *C. elegans* vitellogenins YP170, YP115, and YP88 share sequence homology with vertebrate vitellogenins and with ApoB-100, a core component of mammalian LDL particles (Baker, 1988; Spieth *et al.*, 1991). Endocytosis of yolk particles into membrane-bound vesicles of the oocyte is mediated by receptors of the LDL receptor superfamily in *C. elegans* (this work), insects, and vertebrates. Yolk and yolk receptor endocytic trafficking is thought to proceed through pathways very similar to those used by LDL in somatic cells (Goldstein *et al.*, 1985; Schneider, 1996).

Clathrin-coated pit (CCP) and endosomal trafficking systems, such as those mediating LDL endocytosis, have been intensively studied since Roth and Porter (1964) first discovered coated-pits in the mosquito oocyte plasma membrane. Extensive ligand and receptor tracer studies have since produced a model describing general endocytic trafficking routes in the cell (Mukherjee *et al.*, 1997). Ligand–receptor complexes are thought to cluster in CCPs, which pinch off from the surface as clathrin-coated vesicles, and shed their coats. Uncoated vesicles then fuse with each other and with early endosomes. Acidificaton of the early endosome leads to dissociation of ligands from receptors. After sorting, receptors recycle to the cell surface, whereas ligands are transported to late endosomes and ultimately lysosomes. Yolk storage vesicles are thought to be the oocyte equivalent of late endosomes or lysosomes but with low proteolytic activity (Schneider, 1996).

Although great strides have been made in our understanding of endocytic trafficking, many questions remain about the mechanisms underlying this process. Secretion, which now stands as the best understood trafficking pathway, has been largely elucidated by a combination of mammalian biochemistry and yeast genetics (Rothman and Wieland, 1996; Schekman and Orci, 1996). Endocytosis has been most widely studied by biochemical methods, in large part using physical association or copurification techniques

* Corresponding author. E-mail address: grant@cuccfa.ccc.columbia.edu.

(Mellman, 1996). Some progress has been made using in vitro functional assays, such as early endosome fusion, but many parts of the endocytic pathway, such as receptor recycling, have not been reconstituted (Mukherjee *et al.*, 1997). Genetic analysis in a number of systems, most notably yeast, has also made important contributions to our understanding of endocytosis. For example, genetic analysis in yeast has identified new connections between the actin cytoskeleton and the endocytic pathway (Wendland *et al.*, 1998).

Genetic analysis in metazoan animals such as *C. elegans*, *Drosophila*, and mice is one of the least explored, but potentially most fruitful, areas of endocytosis research. Because endocytosis is a mechanism by which cells interact with their environments, important aspects of endocytosis may differ between unicellular and multicellular organisms. For example, lipoprotein uptake, such as LDL or yolk endocytosis, is an adaptation required for nutrient transport and cellular homeostasis within a multicellular organism. Other highly adapted endocytic systems specific to multicellular organisms include growth factor receptor regulation during development, synaptic vesicle recycling in the nervous system, and antigen processing in the immune system (Mellman, 1996).

Genetic analysis in *C. elegans* and *Drosophila* has already provided important insights into trafficking mechanisms, even though few studies have specifically targeted endocytosis. For instance, mutants in the *Drosophila* dynamin homologue *shibire* were originally identified because of their generally impaired nervous system. Further analysis of these mutants revealed the importance of dynamin in pinching off clathrin-coated vesicles (de Camilli *et al.*, 1995). Similarly, while studying general synaptic function genetically in *C. elegans*, a role for synaptotagmin was identified in synaptic vesicle recycling (Nonet *et al.*, 1993; Jorgensen *et al.*, 1995).

Here, we describe the use of a YP170::green fluorescent protein (GFP) (Chalfie *et al.*, 1994) reporter to visualize yolk endocytosis in vivo in the *C. elegans* oocyte. We used this YP170::GFP assay to probe the functions in yolk endocytosis of predicted *C. elegans* homologues of well-known vertebrate endocytosis genes using RNA-mediated interference (RNAi). This approach showed that the basic components and pathways of endocytic trafficking are well conserved between *C. elegans* and vertebrates, and that this system can be used to test the endocytic functions of any new gene. We also used the YP170::GFP assay in a classical mutagenesis scheme to identify new *rme* (receptor-mediated endocytosis) genes encoding endocytosis components. In this paper we describe RME-2, a member of the LDL receptor superfamily, and provide several lines of evidence showing that RME-2 is the *C. elegans* yolk receptor. The completely described cell lineage, simple anatomy, and advanced knowledge of developmental processes in *C. elegans* offer the potential to integrate future studies of endocytosis and intracellular trafficking with investigations of related processes such as cell polarity, cell–cell signaling, and excitable cell function.

MATERIALS AND METHODS

General Methods and Strains

Methods for the handling and culturing of *C. elegans* were essentially those described by Brenner (1974). All strains were grown at 20°C unless otherwise stated. The wild-type parent for all strains was *C. elegans* var. Bristol strain N2 except for those experiments involving DP13 *C. elegans* var. Bergerac strain BO or NL917 *mut-7(pk204),* a Bristol/Bergerac hybrid strain (Nigon, 1949; Williams, 1995). Mutations used were LGII, *sqt-1(sc103)* (Kramer and Johnson, 1993); LGIII, *mut-7(pk204)* (van Luenen and Plasterk, 1997) and *unc-16(e109)* (Brenner, 1974); LGIV, *dpy-13(e184)* (Brenner, 1974), *unc-5(e53)* (Brenner, 1974), *rme-2(b1005)*, *rme-2(b1008)*, and *rme-2(b1026)* (this work); LGX, *dyn-1(ky51)* (Clark *et al.*, 1997), *lin-15(n765ts)* (Ferguson and Horvitz, 1985), and *bIs1[vit-2::GFP, rol-6(su1006)]* (this work); and unmapped, *bIs2[vit-2::GFP, rol-6(su1006)]* (this work).

Plasmids and Transgenic C. elegans

The plasmid V2B3 encodes a functional VIT-2(YP170B)::GFP fusion protein expressed under *vit-2* promoter control. The plasmid was made by ligating a PCR product encoding *vit-2* genomic sequences, including 1 kb of promoter and the complete gene lacking a stop codon, into the GFP plasmid pPD95.85 (Fire, Xu, Ahnn, and Seydoux, personal communication), cut with *Xma*I and *Kpn*I. The *vit-2* gene was PCR amplified with primers V2F (TCCCCCCGGGTCCACGGACATTTCTGGGTCATTTG) and V2R (CGGGGTACCAGATAAGCGACGCAGGCGGTTGGGAC), containing engineered *Xma*I and *Kpn*I sites (underlined), using cosmid DNA (C42D8) as a template. V2B3, at 50 μg/ml, was coinjected with *rol-6(d)* marker pRF4, at 100 μg/ml, into N2 to make transformed lines using standard methods (Fire, 1986; Mello *et al.*, 1991). Ten of 10 roller lines showed green YP170::GFP fluorescence in embryos, the intestine, and nearly full-grown oocytes of the adult hermaphrodite. Oocyte fluorescence was generally restricted to the one to four late-stage oocytes in each gonad arm, depending on the age of the hermaphrodite. Pseudocoelomic YP170::GFP fluorescence was observed primarily in very young adults just beginning oocyte production or very old hermaphrodites no longer producing fertilized eggs. No expression of YP170::GFP was observed in males. Four integrated lines (*bIs1–bIs4*) were produced by standard methods and back-crossed twice to N2 (Grant and Greenwald, 1997). YP170::GFP fluorescence in the integrated arrays appeared identical to that of the extrachromosomal arrays. *bIs1* was found to map near *dyn-1* on LGX. *bIs2* proved unlinked to *dyn-1* but was not mapped further.

Mutant Isolation and Gene Mapping

Two mutant screens resulted in the isolation of *rme-2* alleles. In the first, 10 gravid hermaphrodites of the mutator strain DH1069 *mut-7(pk204); bIs1[vit-2::GFP, rol-6(su1006)]* were transferred to individual 9-cm Petri dishes and allowed to self-fertilize for 3–4 d, until ~100–200 gravid F1 progeny were produced. F2 eggs were collected by alkaline hypochlorite digestion and were plated in groups of 1000–2000 onto 15-cm Petri dishes. When the F2 progeny reached adulthood, they were examined with a Leica (Nussloch, Germany) 8Z stereomicroscope equipped with epifluorescence for rare animals displaying little or no YP170::GFP fluorescence in the oocytes and embryos but showing bright YP170::GFP fluorescence in the pseudocoelom. Such animals were considered *rme* mutants. True breeding *rme* mutants with morphologically normal gonads were back-crossed first to *unc-16(e109)* to remove *mut-7(pk204)* from the strain. Then an unmutagenized *bIs1* chromosome was crossed back into the strain. Only one mutant from each plate was kept for further analysis. *rme-2(b1005)* and *rme-2(b1008)* were recovered in this screen. The second screen was similar, except that strain DH1006 *bIs1[vit2::GFP, rol-6(su1006)]* was mutagenized with freshly prepared 2.0 mM *N*-ethyl-*N*-nitrosourea as described (De Stasio *et al.*, 1997), and the F1 and F2 generations were raised at 15°C to allow isolation of temperature-sensitive mutants. F2 animals were shifted to 25°C for 12–24 h before screening. *rme-2(b1026)* was recovered in this screen.

Mutations were assigned to linkage groups and to chromosomal subregions by sequence tagged site (STS) polymorphism mapping (Williams, 1995). *b1005*, *b1008*, and *b1026* mapped between stP13 and stP44 on LGIV. These three mutations failed to complement one another. Three-point mapping with *dpy-13* and *unc-5* identified the following crossovers: *dpy-13* (64) *rme-2* (5) and *unc-5*.

Cloning and Molecular Characterization

Genomic *rme-2* sequences were PCR amplified from *rme-2* mutant lysates using primers T11F8-OF (CATTTCTGTCCCGGCGGGAG) and T11F8-OR (ATCGTGCCAAGACCTAGCGCC). The products of four independent PCR reactions were pooled and submitted for automated sequencing using primers T11F8-OF, rme-2F1 (AAGCAAAGGAATTTGATTGCGG), rme-2F2 (TTCTGGAGGAGATGATGAGGTC), rme-2F3 (GTAATGGGATCAAGGAGTGTCC), rme-2F4 (ATCGATCGACTTCATGCATCGC), rme-2F5 (GGCTAATATGGATGGGTCTCAG), rme-2F6 (ACCCATGCCTTGAACTCGAGTG), rme-2F7 (GGTAGTCGGAATTATTGCCTTCC), and rme2-F8 (TCATACGGAAACCCCATGTACG). Sequence changes were confirmed by resequencing the region of interest with a new set of independent PCR products. *rme-2(b1005)* contained a 26-bp deletion altering or deleting codons 630–638 (ATGACCCATpCATCATTCGAGTCCTCAA→A), resulting in a predicted frame shift and truncation. *rme-2(b1008)* contained adjacent missense and single-base insertion mutations within codon 440 (ATT→TGTT), resulting in a predicted frame shift and truncation. *rme-2(b1026)* contained a transition in codon 493 (GGG→GAG) resulting in a nonconservative G→E amino acid substitution.

cDNA clones for *rme-2* were kindly provided by Dr. Yuji Kohara (National Institute of Genetics, Mishima, Japan). The longest, yk8d2, was sequenced on one strand using primers T3, rme-2F2, rme-2F3, rme-2F4, rme-2F5, rme-2F6, rme-2F7, and T7. yk8d2, yk286d10, and yk238g12 each contained a poly(A) tail at the 3′ end, 84 bp after the stop codon.

We determined the 5′ end of the *rme-2* message by 5′ rapid amplification of cDNA ends (RACE) according to the manufacturer's instructions (Life Technologies, Gaithersburg, MD). One microgram of total RNA was reverse transcribed using primer VLDL-RT (CATGAGTTGCACACTCATC) and was poly(G) tailed. First-round PCR was performed using primers VLDL-R1 (CATCGGCAAGCTTATATCCTTC) and the abridged anchor primer. First-round PCR gave only one band on an agarose gel. Second-round PCR was performed using primers rme2-5P (AGTCCGCTACGTTGTCGCATTG) and UAP with a fraction of the first PCR product. Second round PCR gave only one band on an agarose gel. The purified PCR product was cloned into pGEM-T (Promega, Madison, WI). Five of the largest inserts were sequenced. None contained spliced leader sequences. The longest clone extended 35 bp 5′ of the probable start codon. A similar PCR regimen using VLDL-R1 and either SL1 or SL2 primers produced only non–*rme-2*-related products.

Antibody Production, Western Blots, and Immunostaining

Anti-vitellogenin antibodies described by Sharrock *et al.* (1990) were kindly provided by T. Blumenthal (University of Colorado) and S. Strome (University of Indiana). Rat polyclonal antisera anti-YP170, anti-YP115, and anti-YP88 and mouse monoclonal antibodies OIC1 and PIIA3 were used in immunofluoresence experiments on dissected gonads as described below. Each antiserum clearly detected abundant yolk granules in the oocytes of wild-type hermaphrodites but failed to detect any yolk granules in the oocytes of *rme-2(b1005)* hermaphrodites. These antibodies detected abundant yolk in *rme-2* mutant intestines.

We expressed 6-HIS-tagged fragments of RME-2 in *Escherichia coli*, which were purified by nickel chromatography under denaturing conditions, and injected into rabbits for antibody production as described (Grant and Greenwald, 1997). RME-2-EXT antigen (amino acids 180–670) was expressed from a PCR-amplified region of yk8d2 cloned as a *Bam*HI–*Xho*I fragment into pET24b (Novagen, Madison, WI). RME-2-INT antigen (amino acids 813–925) was expressed from a PCR-amplified region of yk8d2 cloned as a *Bam*HI–*Xho*I fragment into pET24b (Novagen). Rabbits R-6739, R-6740, R-6741, and R-6742 were immunized and bled by Charles River PharmServices (Southbridge, MA). Antibodies were affinity purified on RME-2-EXT or RME-2-INT antigen columns as described (Gu *et al.*, 1994). Western blotting was performed on mixed stage populations as described (Grant and Greenwald, 1997), except that affinity-purified anti-RME-2-INT or anti-RME-2-EXT antisera were used at a 1:500 dilution. Whole-mount immunostaining was performed as described (Bettinger *et al.*, 1996). Anti-RME-2 antisera was used at a 1:50 dilution overnight at 4°C. Secondary antibodies conjugated to Alexa-488 (Molecular Probes, Eugene, OR), Alexa-546 (Molecular Probes), or Cy3 (Jackson ImmunoResearch, West Grove, PA) were used at a 1:500 dilution. Gonads were dissected as described (Jones *et al.*, 1996), transferred to siliconized microcentrifuge tubes, and fixed for 10 min in 1% paraformaldehyde and 1× PBS. Primary and secondary incubations were as described above for whole-mount samples. Most immunostained specimens were analyzed with a Zeiss (Thornwood, NY) LSM laser scanning confocal microscope.

Ectopic Expression of RME-2

PCR was used to create plasmid 86DF, a full-length *rme-2* cDNA, including N-terminal coding sequences and a novel *Nhe*I site, cloned into the *Nhe*I and *Kpn*I sites of the *myo-3* expression vector pPD95.86 (Fire, Xu, Ahnn, and Seydoux, personal communication). The complete cDNA was sequenced to ensure that no errors had been introduced. 86DF was injected at 20 μg/ml along with a *lin-15(+)* plasmid at 50 μg/ml into the strain DH1112 *lin-15(n765ts); bIs2[vit-2::GFP, rol-6(d)]*. Three non-Muv lines were grown at 25°C and were fixed and immunostained as described above with rabbit polyclonal anti-RME-2-INT antisera and mouse monoclonal anti-GFP antibody 3E6 (Quantum Biotechnologies, Montreal, Canada). Three of three lines, analyzed by confocal microscopy, showed highly mosaic expression of RME-2 in body wall and vulval muscle cells. In most cases, cells expressing high levels of RME-2 showed coincident staining for YP170::GFP. Because of the small size and presumably active lysosomal degradation pathway of these cells, we were unable to determine whether any of the YP170::GFP associated with these muscle cells was internalized. Muscle cells expressing little or no RME-2, often directly adjacent to strongly positive cells, never stained with anti-GFP antibodies. No anti-GFP immunoreactivity was observed in larvae, although many muscle cells of larvae expressed abundant RME-2 in these lines.

RNA-mediated Interference

The following cDNA clones, kindly provided by Dr. Yuji Kohara or The Institute for Genomic Research (Rockville, MD), were used to produce double-stranded RNA (dsRNA) for microinjection into the pseudocoelom or intestine as described by Fire *et al.* (1998) and Montgomery *et al.* (1998): yk24g12 (clathrin heavy chain, T20G5.1), yk132a1 (α-adaptin, T20B5.1), yk115c10 (β-adaptin, Y71H2), CEESS15 (rab5, F26H9.6), yk101c7 (rab7, W03C9.3), yk51h1 (rab11, F53G12.1), yk52c4 (β'-COP, F38E11.5), yk67d8 (ζ-COP, F59E10.3), and yk112c6 (ARF, B0336.2). Plasmids were rescued from the phage clones according to manufacturer's instructions (Stratagene, La Jolla, CA), the cDNA inserts were PCR amplified with Bluescript vector primers CM024 (TTGTAAAACGACGGCCAG) and CM025 (CATGATTACGCCAAGCTC), transcribed using large-scale T3 and T7 transcription kits (Novagen or Stratagene), and purified by phenol-chloroform extraction or RNA-Quick purification columns (Qiagen, Hilden, Germany). Groups of 15–20 L4 and young adult hermaphrodites of the strain DH1033 *sqt-1(sc103); bIs1[vit-2::GFP, rol-6(d)]* were microinjected with the appropriate dsRNA and allowed to recover 18–24 h before direct observation of oocytes and embryos

within the P0 by fluorescence microscopy. The pseudo–wild-type *sqt-1(0)* mutation *sc103* suppresses the *rol-6(d)* twisted body phenotype, allowing easier observation and photography of this strain. Progeny from the transitional period (first 18–24 h), and fully transformed period (>24 h) were scored in single-day cohorts. For anti-RME-2 immunostaining, groups of 100 P0s were injected, recovered for 24 h, and immunostained as above.

RESULTS

The YP170::GFP Assay

We created transgenic *C. elegans* strains that express the full-length yolk protein YP170 fused to GFP (see MATERIALS AND METHODS). This fluorescent YP170::GFP fusion protein is transported like endogenous yolk, from intestine to oocyte, allowing in vivo analysis of secretion and endocytosis by fluorescence microscopy (Figure 1). In the first set of experiments we asked whether yolk endocytosis in the *C. elegans* oocyte uses the same endocytic pathway components that have been described in studies of general endocytosis in vertebrates. To accomplish this we applied RNAi to our YP170::GFP-expressing strain to reduce or eliminate expression of a series of specific target genes within oocytes (Fire *et al.*, 1998). We then asked whether YP170::GFP uptake by these oocytes was impaired or altered.

RNAi was performed by microinjecting dsRNA homologous to the target gene of interest into L4 or young adult hermaphrodites and later scoring the injected animals and their progeny for induced phenotypes. This technique has been used extensively in *C. elegans* and faithfully mimics most phenotypes caused by mutations that reduce or eliminate target gene function and is especially effective in germ cells (Fire *et al.*, 1998; Montgomery *et al.*, 1998).

Clathrin-coated Pit Components Are Required for Yolk Endocytosis

Both receptor-bound ligands and extracellular fluid enter animal cells through CCPs (Mellman, 1996). The clathrin cage, composed of clathrin heavy chain and clathrin light chain molecules, forms repeated triskelions that self-assemble into planar lattices associated with clathrin adaptor complexes called AP2, which are associated with clustered transmembrane receptors. These planar lattices are thought to round up to form pits, which pinch off from the membrane to form coated vesicles. Another pit-associated protein, dynamin, is required for pinching off clathrin-coated vesicles from the plasma membrane.

The adaptor complex AP2 is a heterotetramer of four "adaptins" (Pearse and Robinson, 1990). Each AP2 complex contains two large subunits, α- and β-adaptin, a medium chain μ2 (AP50), and a small chain σ2 (AP17). The μ2 subunit of AP2 is thought to mediate association with the tyrosine-based internalization signals of receptor tails (Ohno *et al.*, 1995). The α-adaptin subunit is thought to mediate essential interactions, directly or indirectly, with a host of associated endocytosis factors, including dynamin (Wang *et al.*, 1995). The β-adaptin subunit is thought to connect the AP2 complex to clathrin (Pearse and Robinson, 1990). No specific function has been assigned to the σ2 subunit of AP2.

By scanning the essentially complete *C. elegans* genome sequence, we were able to identify predicted *C. elegans* proteins representing probable CCP components: clathrin heavy chain (T20G5.1), α-adaptin (T20B5.1), β-adaptin (Y71H2_389.E), μ2 (R160.1), and σ2 (F02E8.3). *C. elegans* clathrin heavy chain, α-adaptin, and β-adaptin RNAi all produced similar defects in oocytes and embryos. We found that RNAi of these CCP components strongly inhibited uptake of YP170::GFP into oocytes, resulting in high accumulation of YP170::GFP in the pseudocoelomic space and many fewer YP170::GFP-containing yolk granules in late-stage oocytes and embryos. In all of these cases, late-stage oocytes were smaller than in wild type, and embryos proved invia-

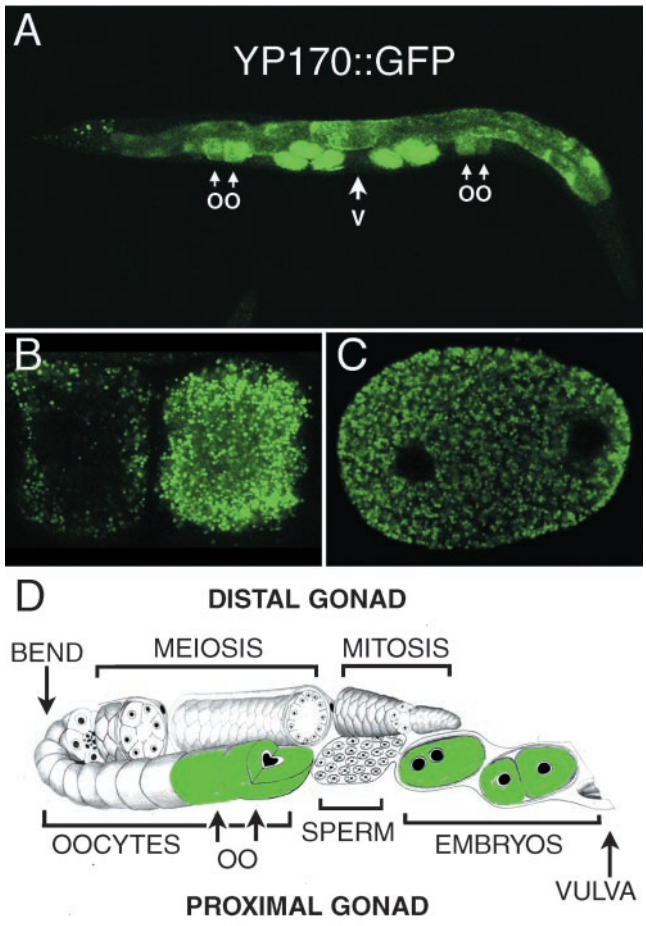

Figure 1. YP170:: GFP accumulates in vesicles of the oocyte. (A) Whole adult hermaphrodite expressing YP170::GFP. YP170::GFP fluorescence is found in the intestine, late-stage oocytes, and embryos. YP170::GFP localization appeared very similar to endogenous YP170 by fluorescence microscopy (this work) and immuno-electron microscopy (Hall *et al.*, 1999). Immuno-electron microscopic experiments did reveal accumulation of YP170::GFP in enlarged vesicles of the intestine, unlike endogenous YP170 in wild-type worms (Hall *et al.*, 1999). Such accumulation may result from overexpression of YP170 in transgenic strains or properties acquired from the GFP tag. OO, late-stage oocytes; V, vulva. (B) Confocal micrograph of YP170::GFP vesicles within two nearly full-grown oocytes of one gonad arm. (C) Confocal micrograph of YP170::GFP vesicles within a two-cell embryo. (D) Stylized drawing of one gonad arm connected to the spermatheca and the uterus.

Table 1. Assay of *C. elegans* endocytosis genes in yolk uptake into the oocyte

Gene targeted for RNAi	Predicted protein homology	% Identity with mammalian homologue	YP170::GFP in pseudocoelom	YP170::GFP in full-grown oocytes	Phenotype of progeny
None	NA	NA	−	+++	Normal
T20G5.1	CHC (Clathrin Heavy Chain)	70	+++	+	Dead embryos
T20B5.1	α-Adaptin	57	+++	+	Dead embryos
Y71H2_389.E	β-Adaptin	53	+++	+	Dead embryos
R160.1	μ2(AP50)	78	−	+++	Strong Dpy
F02E8.3	σ2(AP17)	93	−	+++	Strong Dpy
C02C6.1 (*dyn-1*)[a]	Dynamin	66	+++	+	Dead embryos
F26H9.6	Rab5	77	+++	−	Dead embryos
F53G12.1	Rab11	80	+	++	Dead embryos
				+++	Mild Dpy
W03C9.3	Rab7	71	−	Abnormal localization	Large yolk granules throughout L1 body

[a] Similar results were found for the *dyn-1(ky51ts)* mutant (see RESULTS).

ble. These results are consistent with the proposed roles of clathrin, α-adaptin, and β-adaptin in coated pit and coated vesicle formation.

Unlike the other CCP components we tested, *Ce-μ2*(RNAi) and *Ce- σ2*(RNAi) did not result in an apparent reduction in YP170::GFP uptake into the oocyte. YP170::GFP appeared at wild-type levels in oocytes and embryos and did not accumulate in the pseudocoelomic space. All progeny of *Ce-μ2*(RNAi) and *Ce-σ2*(RNAi) mothers were severely dumpy (Dpy). The Dpy phenotype is characterized by a very short body and is most commonly associated with defects in cuticle formation (Levy *et al.*, 1993). Reduced body length is probably caused by a partial failure in embryonic elongation, a major event in embryonic morphogenesis. The phenotype was very similar when *Ce-μ2* and *Ce-σ2* RNAi was performed simultaneously. No synthetic phenotypes of *Ce-μ2* and *Ce-σ2* were revealed. We also performed RNAi on *Ce-μ2* and *unc-101*, a *C. elegans* μ1(AP47) gene, simultaneously (Lee *et al.*, 1994). No reduction in YP170::GFP uptake by *Ce-μ2*(RNAi); *unc-101(RNAi)* oocytes was observed. We did observe strong Unc and strong Dpy phenotypes in all progeny of these animals, consistent with a simple additive effect of the two dsRNAs. Taken together these results are surprising, perhaps indicating the μ2 and σ2 subunits are not required for yolk endocytosis.

Finally we examined the requirement for *dyn-1*, the *C. elegans* dynamin gene, in YP170::GFP endocytosis by oocytes. We used RNAi and a temperature-sensitive mutation, *dyn-1(ky51ts)*, to reduce or eliminate dynamin function (Clark *et al.*, 1997). *dyn-1*(RNAi) animals and *dyn-1(ky51ts)* mutants, at the nonpermissive temperature of 25°C, showed high-level accumulation of YP170::GFP in the pseudocoelomic space and strongly reduced accumulation of YP170::GFP within oocytes and embryos. *dyn-1*(RNAi) animals produced only dead embryos, whereas *dyn-1(ky51ts)* mutants produced a reduced number of embryos (average = 56; n = 9) at 25°C, 52% of which were inviable. These results are consistent with the proposed role of dynamin in coated vesicle formation.

Endocytic Sorting Pathways Are Required for Normal Yolk Endocytosis

Once molecules have been internalized they enter the endocytic sorting system. Different rab proteins, small GTPases of the ras superfamily, are thought to mediate each unique fusion step in vesicular transport (Mellman, 1996). Genetic studies indicate that rab protein function is often required for vesicle formation as well (Pfeffer, 1994). The rab4 and rab5 proteins are found to associate with early endosomes in mammalian cells. rab4 is important for receptor recycling to the cell surface, whereas rab5 is thought to be required for ligand clustering into coated pits and early endosome fusion (Bucci *et al.*, 1992; van der Sluijs *et al.*, 1992). The rab11 protein associates with early endosomes and the pericentriolar recycling compartment and is thought to be important for transport from early endosomes to pericentriolar recycling endosomes, an important step in recycling for at least some receptors (Ullrich *et al.*, 1996). rab7 protein is associated primarily with late endosomes and is thought to be required for transport of cargo from early to late endosomes (Feng *et al.*, 1995; Press *et al.*, 1998).

We identified three predicted regulators of endosome function, *Ce-rab5* (F26H9.6), *Ce-rab7* (W03C9.3), and *Ce-rab11*(F53G12.1), in the essentially complete genome sequence of *C. elegans* but failed to identify a homologue of rab4. We reduced or eliminated the expression of these predicted endocytosis pathway components by RNAi and examined the resulting defects in the oocytes in a YP170::GFP-expressing strain (see Table 1). Each of these rabs would be expected to regulate a separate step in endocytic trafficking. Indeed, reducing or eliminating expression of each of these rabs produced profound but distinct phenotypes in the *C. elegans* oocyte. Blocking expression of *Ce-rab5* gave results similar to those of CCP component RNAi, except that the phenotype was stronger; i.e. YP170::GFP uptake by oocytes was completely abolished (Figure 2). All progeny embryos of *Ce-rab5*(RNAi) hermaphrodites died.

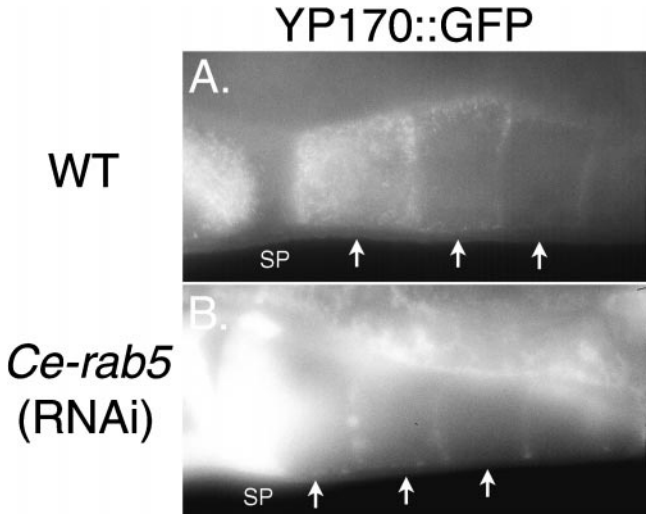

Figure 2. *Ce-rab5*(RNAi) blocks endocytosis of YP170::GFP. (A) Fluorescence micrograph of late-stage wild-type oocytes (arrows). The most full-grown oocyte (far left) is heavily labeled with YP170::GFP vesicles, whereas the two earlier-stage oocytes show less labeling. SP, spermatheca. (B) Fluorescence micrograph of full-grown or nearly full-grown *Ce-rab5*(RNAi) oocytes (arrows). All YP170::GFP fluorescence is found between oocytes, in the spermatheca, pseudocoelom, or intestine. Extremely high levels of extracellular YP170::GFP are seen in the spermatheca (SP). No uptake of YP170::GFP was observed.

Ce-rab11 RNAi had a milder effect on endocytosis by the oocyte. Although YP170::GFP accumulated in the pseudocoelom, indicative of reduced yolk uptake, YP170::GFP accumulation within oocytes and embyos was closer to wild type than after *Ce-chc*(RNAi) or *Ce-rab5*(RNAi) (Table 1). Nevertheless, all embryos produced by *Ce-rab11*(RNAi) hermaphrodites died before hatching.

Although *Ce-rab7*(RNAi) did not appear to significantly impair the uptake of YP170::GFP into oocytes, YP170::GFP was mislocalized in them (see Figure 9M). Rather than small dispersed YP170::GFP vesicles, *Ce-rab7*(RNAi) oocytes contained fewer vesicles of larger size than wild type that were located more peripherally than in wild type. Such vesicles were often an order of magnitude larger than typical yolk granules. We found that newly hatched *Ce-rab7*(RNAi) larvae contained these large yolk vesicles throughout their bodies. Larvae and adult progeny of *Ce-rab7*(RNAi) worms appeared mildly Dpy.

The Secretory Pathway Is Required for Proper Oocyte Formation and Function

Two types of transport vesicles mediate trafficking within the secretory pathway. COPII-coated vesicles mediate transport from the endoplasmic reticulum (ER) to the Golgi apparatus, whereas COPI-coated vesicles are thought to mediate transport within the Golgi and from the Golgi to the ER for recycling of secretory pathway components (Gaynor *et al.*, 1998; Lowe and Kreis, 1998). Some COPI components have also been associated with early endosome function (Daro *et al.*, 1997). Components of both coats have been shown to be required for efficient transport of secreted and membrane proteins to the cell surface (Gaynor *et al.*, 1998).

We reasoned that phenotypes caused by defects in the secretory pathway might indirectly affect endocytosis in the oocyte by preventing newly synthesized yolk receptors from reaching the cell surface. To compare the phenotypic consequences of a general secretory disruption to specific disruption of endocytic function in the oocyte, we performed RNAi on predicted components of the *C. elegans* COPI complex, *Ce-β′*-cop (F38E11.5), *Ce-ζ*-cop(F59E10.3), and *Ce-arf1* (B0336.2).

RNAi of these genes blocked YP170::GFP uptake as expected (Table 2). *Ce-β′*-cop(RNAi), *Ce-ζ*-cop(RNAi), and *Ce-arf*(RNAi) each produced the same array of additional phenotypes, largely distinct from those caused by RNA interference of predicted endocytosis specific genes. Each predicted COPI-coated vesicle RNAi caused many oocytes per gonad arm to take on a rounded appearance with an enlarged nucleus and cytoplasmic streaming, as previously described for mutants defective in the *C. elegans* Sec61p γ homologue (*emo-1*; Iwasaki *et al.*, 1996). Unlike *emo-1*, we observed additional defects: polynucleate oocytes and shellless or weak-shelled embryos that disintegrated in utero or shortly after being laid (Table 2). Such phenotypes could be caused by defects in secretion of membrane required for efficient cytokinesis during oogenesis and by defects in the secretion of eggshell components after fertilization, respectively. These phenotypes were not observed in the endocytic component RNAi experiments. The differences in phenotypes that we observed when endocytic functions were disrupted as opposed to those observed when secretory functions were disrupted will be helpful in distinguishing between mutants defective in one process versus the other. The exceptions will be genes involved in both processes. In such cases we expect defects in the secretory pathway to mask defects in the endocytosis pathway.

Table 2. Requirement for predicted COPI secretory pathway components

Gene targeted for RNAi	Predicted protein homology	% Identity with mammalian homologue	YP170::GFP in pseudocoelom	YP170::GFP in full-grown oocytes	Phenotype of progeny
None	NA	NA	−	+++	Normal
F38E11.5	*β′*-COP	58	+++	−	Dead embryos, abnormal oocytes
F59E10.3	*ζ*-COP	53	+++	−	Dead embryos, abnormal oocytes
B0336.2	ARF1	93	+++	−	Dead embryos, abnormal oocytes

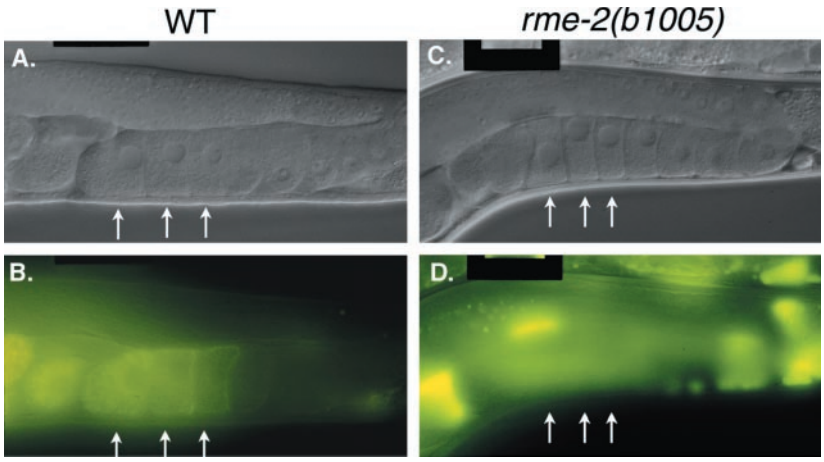

Figure 3. *rme-2* mutants are completely deficient in yolk endocytosis. (A and B) Normarski (A) and fluorescence (B) micrographs of wild-type hermaphrodites expressing YP170::GFP. The three latest-stage oocytes, each with progressively more internalized YP170::GFP, are marked with arrows. (C and D) Nomarski (C) and fluorescence (D) micrographs of *rme-2(b1005)* hermaphrodites expressing YP170::GFP. Note the absence of YP170::GFP in the three latest stage oocytes (arrows) despite the nearly normal morphology of the *rme-2* germ line. All YP170::GFP fluorescence is in the pseudocoelom or in the intestine.

Identification and Phenotype of rme-2

Having validated the YP170::GFP endocytosis assay by the RNAi experiments described above, we set out to use this assay in a mutant screen to identify new genes required for endocytosis. In theory such a mutant screen could identify genes specifically required for yolk endocytosis as well as general factors required for all endocytosis. Here we describe the identification of the *C. elegans* yolk receptor as an example of the effectiveness of this genetic screen in identifying components of the oocyte endocytosis pathway.

We predicted that mutants defective in endocytosis would produce morphologically wild-type oocytes and early embryos devoid of YP170::GFP, and that high levels of YP170::GFP would accumulate in the pseudocoelom of such mutants. Our prediction that endocytosis-defective oocytes and early embryos would appear nearly wild-type by Nomarski optics was based on our RNAi studies of endocytosis genes and studies of the *dyn-1* mutant. In addition, studies of sex determination mutants in *C. elegans* showed that oocytes produced in intersex animals, lacking yolk production, have nearly normal morphology (Doniach and Hodgkin, 1984). Therefore, we screened the F2 generation of a mutagenized YP170::GFP-producing strain for adult hermaphrodites, which contained normal-appearing oocytes that were refractory to YP170::GFP endocytosis. Such mutants show a characteristic accumulation of YP170::GFP fluorescence in the pseudocoelomic space, outlining the internal organs, with reduced or absent YP170::GFP fluorescence in the oocytes and embryos. We isolated three mutant alleles constituting one complementation group, *rme-2*, in which oocytes of normal appearance are produced but are completely devoid of YP170::GFP fluorescence (Figure 3). The other 11 *rme* genes identified in this screen will be described elsewhere.

rme-2 mutants are characterized by slightly small oocytes devoid of yolk, otherwise normal germ line morphology, high-level pseudocoelomic yolk accumulation, reduced embryo production, and low embryo viability. We find that *rme-2* mutant oocytes lack any detectable endogenous yolk proteins, as assayed by immunofluorescence, including YP170A, YP170B, YP115, and YP88 (see MATERIALS AND METHODS). Embryo production is reduced in *rme-2* mutants to an average of 78 (n = 47) compared with ~300 in wild type. Damaged oocytes and embryos are found in the uterus of *rme-2* mutant hermaphrodites, consistent with a defect in ovulation. Defects in ovulation, such as those found in endomitotic (*emo*) mutants, cause some oocytes to become fragmented by premature closure, or failure to open, the spermathecal valve (Clandinin *et al.*, 1998; McCarter *et al.*, 1999). Time-lapse video recordings of *rme-2* mutant ovulations, performed by Tim Schedl (personal communication), indicate a frequent failure of spermathecal dilation as well as common premature closure, which breaks passing oocytes into fragments. A high percentage of *rme-2* gonad arms contain one endomitotic-like oocyte proximal to the spermatheca (Schedl, personal communication). Most *rme-2* mutant embryos fail to hatch (viability, 23%). Embryos that hatch proceed through normal larval development to produce adult animals with the defects described above.

Molecular Characterization of rme-2

We mapped *rme-2* to a position very close to the left of *unc-5* on LGIV (see MATERIALS AND METHODS). Upon examination of the predicted genes in this region (*C. elegans* Sequencing Consortium, 1998), we noticed T11F8.3, a gene that could encode a receptor of the LDL receptor (LDLR) superfamily. Because yolk receptors from insects and vertebrates are members of the LDLR superfamily, we reasoned that *rme-2* and T11F8.3 might be the same gene (Stifani *et al.*, 1990; Schonbaum *et al.*, 1995). This hypothesis was strengthened by our subsequent finding that T11F8.3(RNAi) produced phenotypes very similar to those found in *rme-2* mutants, including late-stage oocytes and early embryos devoid of YP170::GFP. Sequencing of the T11F8.3 gene from each *rme-2* mutant revealed a unique DNA sequence change, which alters the predicted protein product (See below). These results indicate that *rme-2* corresponds to the predicted gene T11F8.3.

We determined the sequence of a nearly complete *rme-2* cDNA clone, yk8d2. We also determined the 5′ end of the *rme-2* mRNA by 5′ RACE. Several RACE products were sequenced, the longest of which extended 153 bp farther 5′ than yk8d2, 35 bases 5′ of a likely AUG start codon. This AUG is the first of the open reading frame and directly precedes a predicted hydrophobic amino acid sequence with features of a secretory signal sequence (von Heijne, 1986).

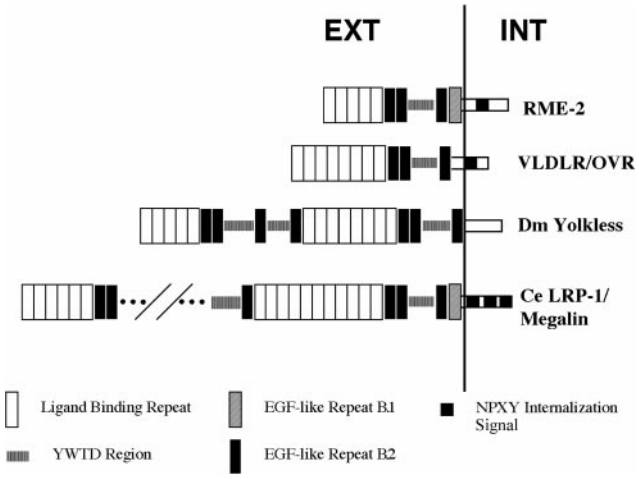

Figure 4. RME-2 is a member of the LDLR superfamily of lipoprotein receptors (GenBank accession number AF185706). Repetitive motifs shown include acidic ligand-binding sequences with six cysteines each, EGF-like repeats with six cysteines each (B.1 and B.2 type; Herz *et al.*, 1988), YWTD repeats, which are thought to form a β-propeller structure (Springer, 1998), and the consensus internalization signal FDNPXY. VLDLR/OVR, very low-density lipoprotein receptor (Gafvels *et al.*, 1993)/chicken yolk receptor (Shen *et al.*, 1993); Dm Yolkless, *Drosophila* yolk receptor (Schonbaum *et al.*, 1995); Ce LRP-1/Megalin, *C. elegans* megalin gene product (Yochem and Greenwald, 1993). Only a partial map of *lrp-1* motifs is shown because of its large size. For a complete description, see Yochem and Greenwald (1993).

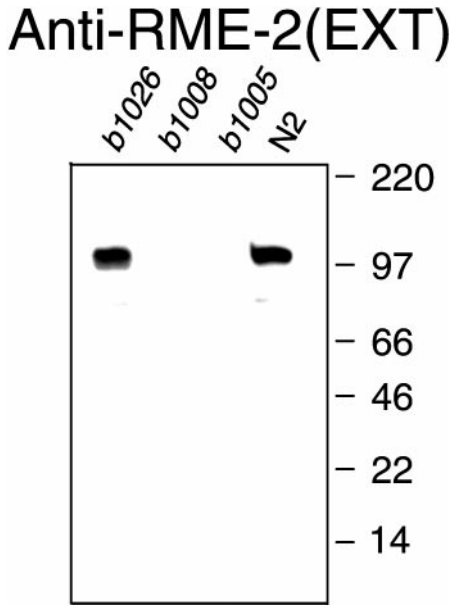

Figure 5. RME-2 Western blot. Total *C. elegans* proteins were size separated by SDS-PAGE, transferred to a polyvinylidene difluoride membrane, and probed with anti-RME-2(EXT) affinity-purified antibodies. Identical results were observed with anti-RME-2(INT) affinity-purified antibodies (our unpublished findings). Equal protein loading was confirmed by Coomassie blue staining of duplicate gels (our unpublished findings).

No evidence for a trans-spliced leader on *rme-2* messages was obtained. A combination of cDNA and RACE product sequencing indicated a full-length *rme-2* mRNA size of 2.9 kb. Northern analysis of poly(A)$^+$ and total RNA from mixed stage N2 worms confirmed the presence of a single *rme-2* mRNA species of ~2.9 kb (our unpublished findings).

RME-2 is an LDLR Family Member

The predicted *rme-2* protein is 925 amino acids in length, containing several repeated sequence motifs, with overall similarity to members of the LDLR superfamily of lipoprotein receptors (Figure 4). Hydropathy analysis indicates two highly hydrophobic sequences within RME-2. The first hydrophobic sequence is a likely N-terminal secretory signal sequence, whereas the second located near the C terminus is a likely transmembrane domain. These findings are consistent with a typical type I transmembrane protein topology, with a large N-terminal extracellular domain and a short (110 aa) intracellular domain. C-terminal to the predicted signal sequence are five tandem class A ligand-binding repeats, each containing six cysteine residues with characteristic spacing and typical anionic SDE or DDE sequences (Esser *et al.*, 1988). These are followed by two predicted class B EGF-like cysteine-based repeats (Sudhof *et al.*, 1985). The EGF-like repeats are followed by an intervening region of so-called YWTD repeats, which have been predicted to produce a sixfold symmetrical β-propeller structure (Springer, 1998). Between the YWTD region and the predicted transmembrane domain we find two more class B EGF-like repeats. Finally, within the predicted intracellular domain we find a single predicted internalization signal of the NPXY type (Chen *et al.*, 1990).

We sequenced PCR products including the complete coding region of the *rme-2* gene from each *rme-2* mutant. Both *rme-2(b1005)* and *rme-2(b1008)* contained DNA sequence alterations producing predicted truncations of the *rme-2* protein, deleting part of the YWTD region, EGF-like repeats 3 and 4, and the predicted transmembrane and intracellular domains. Such mutated proteins are unlikely to retain any endocytic function and are predicted null alleles. *rme-2(b1026)* contained a single nucleotide transition, resulting in a nonconservative amino acid substitution, G→E, in the fourth predicted YWTD repeat.

Analysis of the rme-2 Protein

To analyze the *rme-2* protein, we produced affinity-purified polyclonal antisera specific for the predicted extracellular (anti-RME-2-EXT) and intracellular (anti-RME-2-INT) domains of RME-2 (see MATERIALS AND METHODS). Western blots of total protein from mixed stage populations probed with either anti-RME-2 antiserum showed a single band of ~110 kDa, very close to the predicted size for RME-2 (Figure 5). No protein bands were detected with either anti-RME-2 antisera in lanes containing protein from *rme-2(b1005)* or *rme-2(b1008)* mutants, indicating the specificity of the antisera (Figure 5).

We examined the expression pattern of RME-2 in whole-mount mixed populations, mixed stage embryo populations, and dissected adult hermaphrodite gonad preparations by

immunofluorescence using our specific anti-RME-2 antisera. We found abundant RME-2 in the proximal germ line of adult hermaphrodites and within all cells of early embryos. We failed to detect RME-2 in any other cells (see MATERIALS AND METHODS).

The adult hermaphrodite gonad consists of two ovaries connected to a central uterus and two spermathecae (Figure 1D). Eggs are laid through the vulva, a ventral opening in the body wall connected to the uterus. Each ovotestis is a reflexed tube with a vulva proximal and vulva distal arm connected by a bend region. The distal arm contains immature germ cell nuclei, with partial plasma membranes, connected by a shared central cytoplasm. Mitotic nuclei are found at the extreme distal end. As germ cells progress in the proximal direction they enter meiosis, reaching diplotene of meiotic prophase I near the bend. In the loop region germ cells become partitioned into individual cells and become differentiated oocytes, increasing in size as they approach the spermatheca and uterus.

RME-2 expression appears to be an early event in oocyte differentiation. Within the germ line, RME-2 first becomes detectable within germ cells in the bend region of the gonad arm. RME-2 first appears in these cells in cytoplasmic puncta reminiscent of vesicles. In later-stage oocytes anti-RME-2 antibodies stain many prominent puncta at or near the plasma membrane in addition to the intracellular puncta (Figure 6B).

As the oocytes grow, they begin to accumulate yolk proteins taken up from the pseudocoelom. The uptake of YP170::GFP into oocytes coincides with the appearance of RME-2 on or near the cell surface (Figure 6A). In nearly full-grown oocytes of a gonad arm, cytoplasmic localization of RME-2 is reduced, and prominent cell surface staining appears. Much of the RME-2 detected by immunostaining in late-stage oocytes appears to be clustered at or near the cell surface, consistent with being localized to CCPs or plasma membrane proximal endosomes (Figure 6, E and H).

Wild-type embryos gave a very different immunostaining pattern from oocytes. All cells of early embryos display prominent anti-RME-2 immunostaining in abundant intracellular vesicular structures but lack any apparent RME-2 in the plasma membrane (Figure 6J). At the earliest time points in embryogenesis we were able to examine (see MATERIALS AND METHODS), all RME-2 was found in these intracellular vesicles. Therefore, this redistribution of RME-2 from the cell surface to intracellular vesicles appears to occur sometime shortly after ovulation, perhaps coincident with the dramatic cellular changes associated with fertilization. As the embryos develop, the number of anti-RME-2–reactive vesicles diminishes, until by hatching little or no RME-2 is detected. The gradual disappearance of RME-2 from these vesicles may indicate degradation in a lysosome-like compartment. We did not find evidence of new RME-2 expression during embryogenesis.

Each of the three *rme-2* mutants displays aberrant gonadal immunostaining patterns with anti-RME-2 antisera. Both mutants predicted to produce truncated versions of RME-2, *rme-2(b1005)* and *rme-2(b1008)*, fail to stain with antisera specific for the RME-2 intracellular domain, and both display very weak or no immunostaining with antisera specific for the RME-2 extracellular domain (Figure 7). Residual staining in these mutants detected with anti-RME-2-EXT antisera is diffuse and is not clearly localized to the oocyte surface membranes. The YWTD missense mutant *rme-2(b1026)* produces abundant cytoplasmic immunostaining with both anti-RME-2 antisera but lacks defined RME-2 localization at the oocyte plasma membrane (Figure 7). Because *rme-2(b1026)* contains a missense mutation in its extracellular domain, it may be recognized by the ER quality control machinery as misfolded and prevented from exiting the ER. This effect is commonly found with misfolded proteins passing through the ER. Such ER retention has been seen before in *C. elegans* in the case of a mutant GLP-1 receptor (Wen and Greenwald, 1999).

RME-2 Is Sufficient to Induce YP170::GFP Binding

If *rme-2* encodes the *C. elegans* yolk receptor, as indicated by its mutant phenotype and LDLR homology, then ectopic expression of RME-2 in cell types other than the oocyte should lead to the association of yolk with such cells. We tested this hypothesis by expressing RME-2 in body wall muscle cells using the *myo-3* promoter (Okkema *et al.*, 1993) and checked these transgenic animals for localization of YP170::GFP to RME-2-expressing muscle cells. In these strains body wall muscle cells expressing high levels of RME-2, as assayed by anti-RME-2 immunostaining, showed significant surface accumulation of YP170::GFP, whereas adjacent muscle cells expressing little or no RME-2 did not accumulate YP170::GFP (Figure 8). Thus, expression of RME-2 in these cells is sufficient to direct the specific binding of yolk particles. We were unable to determine whether YP170::GFP was internalized by RME-2-expressing muscle cells (see MATERIALS AND METHODS).

Endocytic Trafficking of RME-2 in the Oocyte

We wished to determine directly the importance of some of the general endocytosis factors described above in RME-2 endocytic cycling and to help establish whether YP170::GFP and RME-2 cosegregate through parts of the endocytic pathway as expected for a ligand–receptor pair. To accomplish these goals we analyzed the subcellular localization of the RME-2 yolk receptor in oocytes by immunofluorescence after RNAi of a select group of general endocytosis genes.

We found that oocytes from *Ce-chc*(RNAi) animals displayed higher than wild-type accumulation of RME-2 at the oocyte cell surface and showed a concomitant reduction in cytoplasmic RME-2 staining (Figure 9). YP170::GFP and RME-2 colocalized at the oocyte surface. Furthermore, we observed that the prominent RME-2 puncta at or near the surface of wild-type oocytes were reduced or missing in *Ce-chc*(RNAi) oocytes. Instead, surface RME-2 staining appeared diffuse (Figure 9). Like the *Ce-chc*(RNAi), *Ce-rab5*(RNAi) resulted in RME-2 localization at or near the cell surface of the oocyte. RME-2 immunostaining appeared diffuse, failing to produce prominent puncta (our unpublished findings). *Ce-rab11*(RNAi) resulted in RME-2 immunofluorescence near the cell surface appearing more punctate, with some of the puncta taking on a tubular or mesh-like appearance (Figure 9). *Ce-rab11*(RNAi) did not result in colocalization of YP170::GFP and RME-2. *Ce-rab7*(RNAi) oocytes showed reduced RME-2 accumulation at or near the oocyte surface. Surface-proximal RME-2 displayed a normal distribution of puncta (our unpublished findings). Unexpectedly, *Ce-rab7*(RNAi) oocytes showed prominent accumulation of

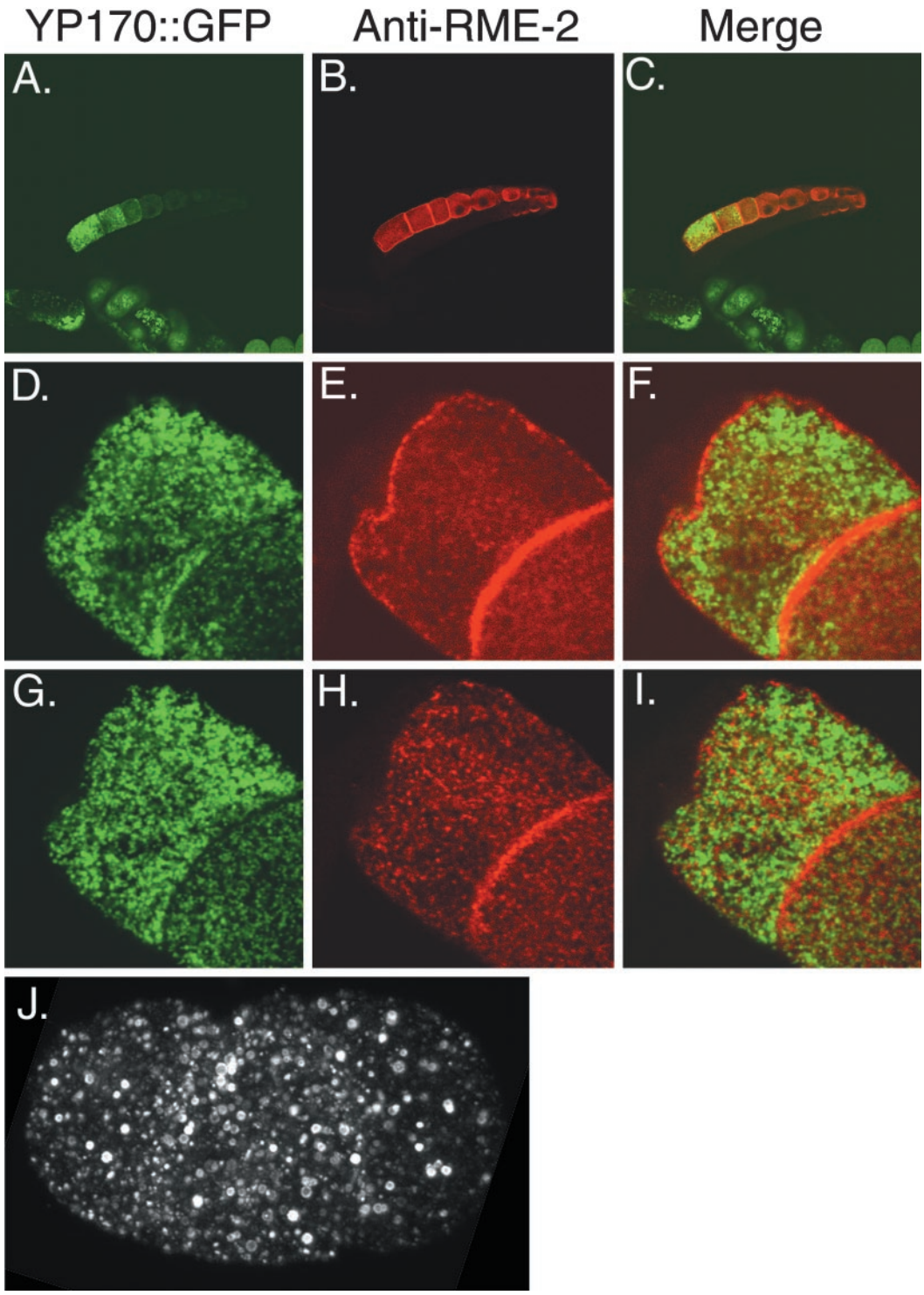

Figure 6. Localization of RME-2 in the gonad and embryo of a YP170::GFP-expressing strain. (A–C) Confocal micrographs of a dissected gonad, showing YP170::GFP (green) and anti-RME-2 (red). Embryo and intestine YP170::GFP fluorescence is evident at the bottom of A and C. Embryos in B do not stain with anti-RME-2 antibodies, because their eggshells are not permeablized by the procedure used to fix and stain the dissected gonad. High-magnification (3000×) confocal micrographs of full-grown oocytes in a middle focal plane (D–F) or top focal plane (G–I) show abundant YP170::GFP and anti-RME-2 immunofluorescence. RME-2 and YP170::GFP signals do not appear to colocalize at steady state. RME-2 immunoreactivity patterns are very different in embryos. All RME-2 appears intracellular in the four-cell embryo (J) and declines progressively during embryogenesis.

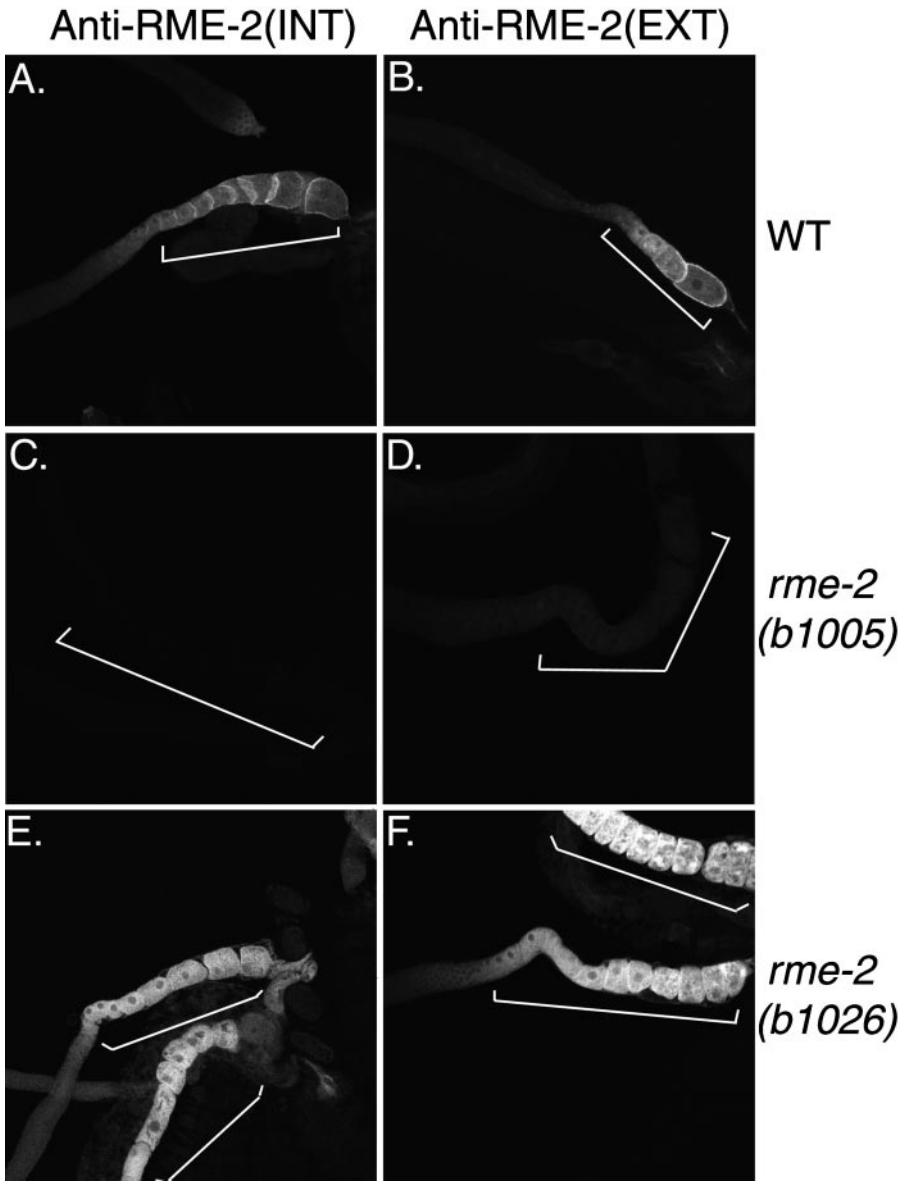

Figure 7. Anti-RME-2 immunostaining of *rme-2* mutants. (A and B) Confocal micrographs of wild-type dissected gonads stained with antibodies to the RME-2 intracellular and extracellular domains, respectively. Micrographs were produced using identical scan settings, allowing direct comparison of fluorescent intensities. Oocytes are indicated by brackets. Differences in staining in A and B result from differences in gonad age rather than differences in immunofluoresence pattern between antisera. The gonad in B is from a young adult, whereas that in A is from an older adult. (C and D) *rme-2(b1005)* mutant oocytes failed to stain with anti-RME-2(INT) antibodies (C) and showed very little reactivity to anti-RME-2(EXT) antibodies (D). *rme-2(b1008)* mutant oocytes gave very similar results (our unpublished findings). (E and F) *rme-2(b1026)* mutant oocytes showed strong anti-RME-2 immunofluorescence throughout the cell, possibly indicating ER retention.

RME-2 to the same large peripheral vesicles that accumulated YP170::GFP (Figure 9). By analogy to mammalian systems we expect these large vesicular structures to be early endosomes. Accumulation of RME-2 in early endocytic structures in *Ce-rab7*(RNAi) oocytes may indicate a role for *Ce-rab7* in receptor recycling. Colocalization of YP170::GFP and RME-2 to the same endocytic structures in *Ce-rab7*(RNAi) oocytes is consistent with their identification as a ligand–receptor pair.

DISCUSSION

Yolk Endocytosis: In vivo Endocytic Trafficking in C. elegans

We have developed an in vivo visual assay for the uptake and trafficking of an endocytic ligand, YP170::GFP, by growing oocytes. We tested the importance of conserved components of the general endocytosis pathway for YP170::GFP endocytosis by RNA-mediated interference and found that components of conserved sequence showed conservation of function as well. This new assay system has also allowed us to perform mutant screens to identify new genes required for endocytosis. We expected to identify genes specifically required for yolk uptake, such as the *rme-2* gene described here, as well as genes required for endocytosis in many or all cell types. Preliminary analysis of other *rme* mutants identified in the same screen indicates that many are required more generally for endocytic trafficking (Grant, Hirsh, Pedraza, and Zhang, unpublished observations). Together these experiments describe a general system for reverse and forward genetic analysis of endocytosis in *C. elegans*.

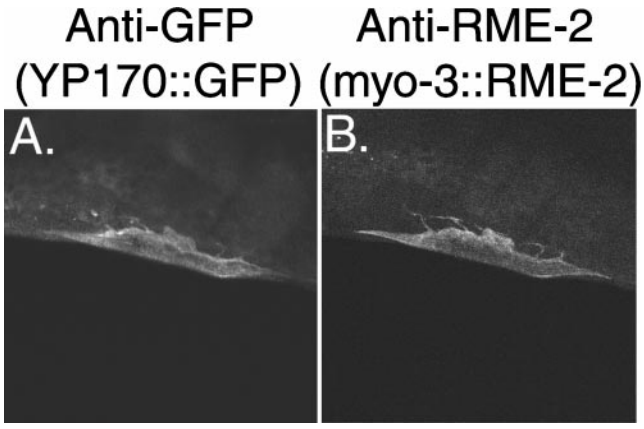

Figure 8. Ectopic expression of RME-2 induces ectopic binding of YP170::GFP to RME-2-expressing cells. Shown is anti-GFP (A) and anti-RME-2 (B) immunolabeling of an adult hermaphrodite body wall muscle cell in a strain of the genotype *lin-15(n765); bIs1[vit-2::gfp, rol-6(d)]; Ex[myo-3::rme-2, lin-15(+)]*.

RME-2: The C. elegans Yolk Receptor

We propose that RME-2 is the *C. elegans* yolk receptor based on its mutant phenotype, expression pattern, molecular nature, and sufficiency to induce yolk binding in a heterologous cell type. Yolk receptors from insects and vertebrates have been cloned in recent years (Schneider, 1996; Sappington and Raikhel, 1998). All of them are members of the LDLR superfamily of lipoprotein receptors. They vary in size, mainly in their extracellular domains, differing in the number of class A ligand-binding repeats (LRs), class B EGF-like repeats, and YWTD repeat regions (Schneider, 1996). The chicken and *Xenopus* yolk receptors, like the human VLDL receptor, are eight ligand-binding repeat, or LR8, members of this family and contain typical NPXY internalization motifs in their intracellular domains (Schneider, 1996). The yolk receptors of mosquito and *Drosophila* are LR13 receptors, with class A repeats divided into an N-terminal group of five and a more membrane-proximal group of eight. Each of these lacks a consensus NPXY signal but instead contains likely dileucine internalization signals (Sappington and Raikhel, 1998). The *C. elegans rme-2* gene is the first LR5 member of the LDLR gene family and contains a typical NPXY internalization signal like its vertebrate cousins. It would be interesting to test the affinity of *C. elegans*, mosquito, and *Drosophila* yolk receptor N-terminal five class A repeat clusters for yolk binding, because they are unique among the known LDLR superfamily members.

The *C. elegans* genome contains several other members of the LDLR superfamily, including an LR8 (T13C2.4; Springer, 1998), and two very large receptors related to megalin (*lrp-1*) and LRP (F47B3.8/T21E3.3). Of these, only *lrp-1* has been characterized genetically. LRP-1 is expressed primarily in the hypodermis, and *lrp-1* mutants are larval lethals with apparent molting defects (Yochem *et al.*, 1999). No evidence was found for genetic redundancy between *rme-2* and *lrp-1* in double mutant strains (Yochem, personal communication). Further analysis by *C. elegans* genetics is likely to reveal more important information about the roles of this conserved metazoan gene family in cellular homeostasis and development.

Yolk Trafficking in the Embryo

After fertilization, yolk granules are segregated approximately equally among progeny blastomeres. Yolk proteins appear to be metabolized slowly during embryogenesis, with many yolk granules remaining in newly hatched larvae. At hatching most of the remaining yolk is found in cells of the intestine. Bossinger and Schierenberg (1992, 1996) showed that selective secretion and reuptake, rather than selective segregation or degradation, are responsible for the visible change in yolk distribution during embryogenesis. Around midembryogenesis, nonintestinal cells resecrete most of the yolk particles they inherited from the oocyte. This resecreted yolk accumulates briefly in the perivitelline space and is then taken up into new storage vesicles by embryonic intestinal cells. One reasonable hypothesis would be that the same receptor responsible for yolk uptake into oocytes from the pseudocoelom would also function in the embryonic intestine for this second uptake event. However, close examination of the RME-2 expression patterns with anti-RME-2 antibodies failed to reveal evidence for RME-2 endocytic function during embryogenesis. In mammals oxidized LDL is taken up by a different receptor than regular LDL. The receptor for oxidized LDL is a member of the lectin family (Sawamura *et al.*, 1997). The *C. elegans* genome contains many genes encoding proteins similar to lectin-type receptors (Grant, unpublished observation). Perhaps one or more of these receptors is involved in the uptake of yolk into the embryonic intestine.

We have observed that most YP170::GFP remaining in newly hatched larvae is in the intestine, indicating that this fusion protein also undergoes embryonic transport like endogenous yolk. We have also observed that blocking a late transport step in YP170::GFP uptake into the oocyte, by *Ce-rab7*(RNAi), leads to ectopic localization of enlarged yolk granules throughout the body of newly hatched larvae (our unpublished findings). This may indicate that yolk granules formed from an early endocytic compartment, as opposed to a late endocytic compartment, are not competent for resecretion during embryogenesis. Perhaps this process of resecretion is analogous to the regulated secretion of lysosomal contents by mammalian cells (reviewed by Page *et al.*, 1998) and would be amenable to genetic analysis in *C. elegans*.

General Endocytic Trafficking Factors

Yolk endocytosis systems in many organisms have been compared with the best studied endocytosis pathway, that of mammalian LDLs (Goldstein *et al.*, 1985). The homology between mammalian ApoB-100 and the vitellogenins as well as that between LDLR and the known vitellogenin receptors has prompted the hypothesis that the mammalian LDL uptake pathway is the most recent modification of the ancient yolk endocytosis apparatus (Schneider, 1996). Like the LDL uptake pathway, vitellogenin receptors bound to yolk particles are thought to be internalized by clathrin-coated vesicles, which uncoat and fuse to form early endosomes. Unlike somatic cells, oocytes are thought to lack lysosomes per se and their high proteolytic capacity (Schneider, 1996). Yolk remains stored in an endosomal compartment, probably equivalent to lysosomes until used during embryogenesis.

The complete genome sequence of *C. elegans* and the facile reverse genetic technique of RNA-mediated interference al-

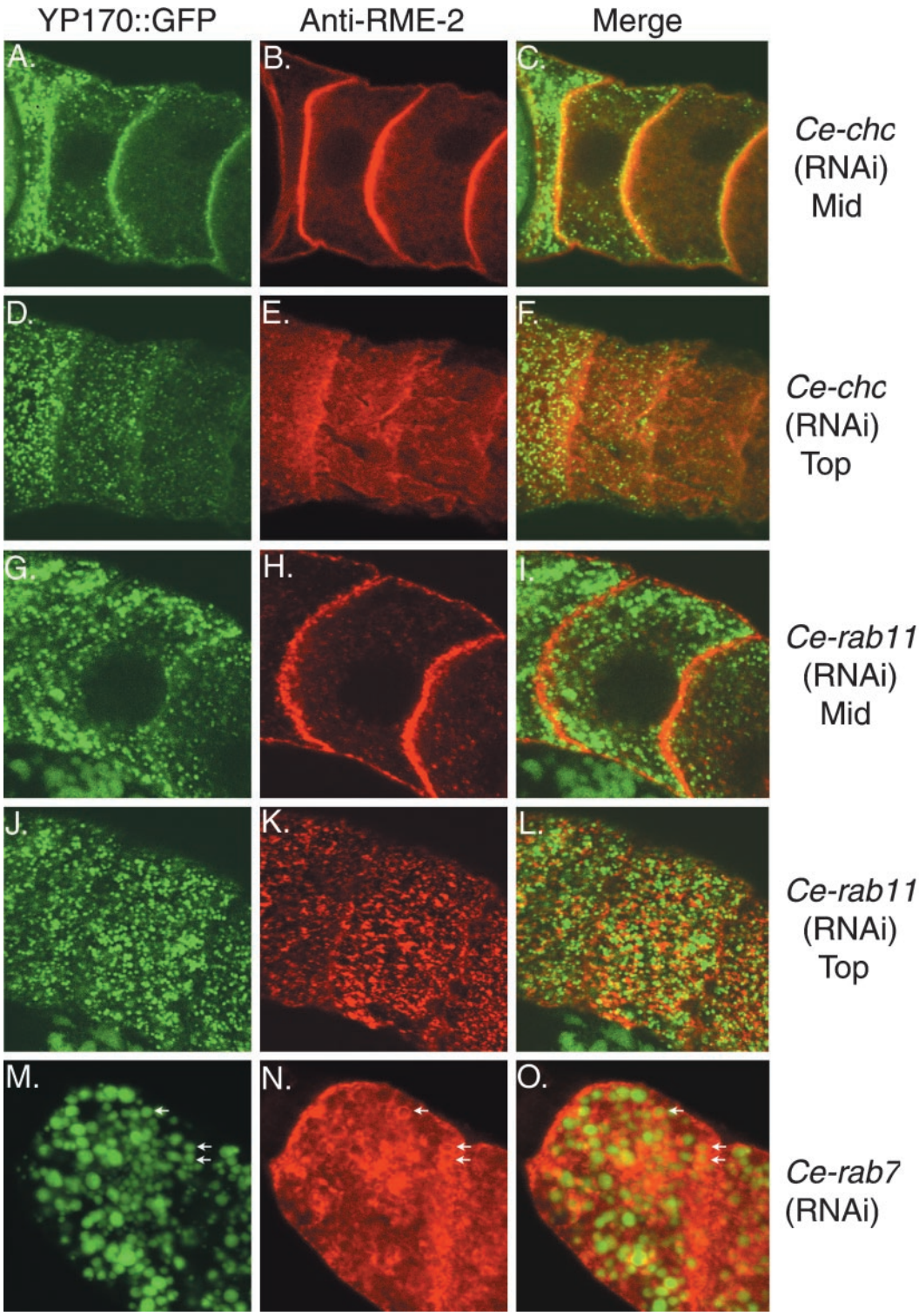

Figure 9. YP170::GFP and RME-2 localization after RNAi of certain endocytosis factors. Confocal micrographs of oocytes in dissected gonads from RNAi animals show YP170::GFP fluorescence (green) and anti-RME-2 immunostaining (red). Mid, middle focal plane; Top, top focal plane. *Ce-clathrin heavy chain (Ce-chc)* RNAi (A–C) resulted in accumulation of YP170::GFP and RME-2 at the cell surface and more diffuse surface anti-RME-2 staining (E) than wild type (Figure 6). *Ce-rab11*(RNAi) oocytes showed reduced internalized YP170::GFP (G) and more punctate, less diffuse RME-2 staining (H and K) than wild-type. *Ce-rab7*(RNAi) oocytes showed YP170::GFP accumulation in large peripheral vesicles (M) and RME-2 accumulation (N) in these same large vesicles. Some of the vesicles containing both YP170::GFP and RME-2 are marked with arrows.

lowed us to test some of these hypotheses in our YP170::GFP uptake assay. In general our results correlated well with the predicted order of events in the yolk uptake pathway of *C. elegans*. *C. elegans* homologues of CCP components were clearly important for yolk uptake, as was the *C. elegans* homologue of the early endosomal regulator rab5. *Ce-chc*(RNAi) and *Ce-rab5*(RNAi) induced accumulation of ligand (YP170::GFP) and receptor (RME-2) together at or near the oocyte surface. In both cases RME-2 immunofluoresence at or near the cell surface appeared diffuse, lacking the characteristic punctate pattern typical of wild-type oocytes and might represent diffuse plasma membrane localization. Although we currently cannot identify the RME-2 membrane-proximal puncta as cell surface structures such as pits or subsurface structures such as endosomes, either might be expected to lack RME-2 after depletion of clathrin or rab5. Interestingly, a role for rab5–guanine nucleotide dissociation inhibitor complexes in sequestration of ligand–receptor complexes into CCPs, in addition to the well-studied function of rab5 in endosome fusion, was recently shown (Horiuchi *et al.*, 1997; McLauchlan *et al.*, 1998). Our results are consistent with uptake of vitellogenin–RME-2 complexes through CCPs and early endosomes.

In these RNAi experiments, the only predicted CCP components that did not appear to be required for YP170::GFP endocytosis were *Ce-μ2* and *Ce-σ2*. Alone or in combination, RNAi for these genes produced only one phenotype, extremely Dpy progeny. This result is quite surprising, because μ2 is thought to provide the primary link between receptors and the internalization machinery (Ohno *et al.*, 1995). In addition, clathrin adaptor complexes are thought to become unstable if one component of the tetramer is compromised, implying that removal of any one subunit should give the same phenotypes (e.g., Dell'Angelica *et al.*, 1999).

One interesting interpretation of these results would be that *Ce-μ2* and *Ce-σ2* are not required for yolk endocytosis, or viability, unlike *Ce-α*-adaptin and *Ce-β*-adaptin. The similar Dpy phenotypes displayed in *Ce-μ2*(RNAi) and *Ce-σ2*(RNAi) animals may indicate defects in hypodermal development. Perhaps medium or small chains from other adaptin complexes in the worm (e.g., AP1 and AP3) can partially substitute for *Ce-μ2* and *Ce-σ2*, as suggested by some overlap in the in vitro affinities of medium chains for sorting signals (Ohno *et al.*, 1998). We did not find evidence for functional redundancy between *Ce-μ2* and *unc-101*, a *Ce-μ1*. Another possibility is that the RNAi technique did not sufficiently reduce *Ce-μ2* and *Ce-σ2* function to reveal their null phenotypes. If this is the case, we might have expected *Ce-μ2*(RNAi); *Ce-σ2*(RNAi) to show additional defects. Again, these experiments failed to reveal a role for *Ce-μ2* and *Ce-σ2* in yolk endocytosis. Full exploration of these possibilities awaits the isolation and analysis of *Ce-μ2* and *Ce-σ2* null mutants.

The *Ce-rab11*(RNAi) phenotype was consistent with a role for receptor recycling in yolk endocytosis: YP170::GFP uptake was reduced, and RME-2 localization was altered. RME-2 accumulated in surface-proximal structures that appeared more numerous, enlarged, and less regular than puncta prominent in wild-type oocytes. These results are consistent with possible accumulation of RME-2 receptors in early endosomal or recycling structures. We searched the *C. elegans* genome for rab11 and rab4, regulators of receptor recycling. We found a second gene (W04G5.1) homologous to rab11 but none closely related to rab4. Because of the sequence similarity to one another (80% identical at the mRNA level), it is possible that RNAi against one *Ce-rab11* would interfere with expression of both (Fire *et al.*, 1998). Perhaps one or both rab11 homologues serve functions similar to rab4 in mammalian cells.

In mammalian cells rab7 is thought to be required for transport from early to late endosomes (Feng *et al.*, 1995). Mammalian tissue culture cells, expressing a dominant negative form of rab7, accumulate cell surface molecules traversing the endocytic route from cell surface to the lysosome in enlarged early endosomes. We have blocked expression of *Ce-rab7* by RNAi and observed accumulation of YP170::GFP in large peripheral vesicles of the oocyte, a phenotype very similar to that described above for mammalian cells (Figure 9).

Unexpectedly, we also observed significant accumulation of the putative receptor, RME-2, in these same large peripheral vesicles of oocytes depleted of *Ce-rab7* activity. Expression of dominant negative Rab7 protein was not found to interfere with recycling of receptors from the early endosome to the cell surface in mammalian cells (Feng *et al.*, 1995). Because a large volume of yolk is taken up into oocytes in a relatively short period, and because RME-2 is similar to the rapidly recycled LDLR, it seems likely that RME-2 recycles frequently during oogenesis. Because we do not see RME-2 accumulating in the same storage vesicles as yolk particles in wild-type oocytes, it seems likely that yolk and yolk receptor are sorted from one another after internalization. After sorting, the receptors could be recycled or degraded.

Because oocytes are thought to have very low degradative capacity, we consider two simple models of RME-2 recycling as likely scenarios that could account for these observations. First, RME-2 could be rapidly recycled from early endosomes, in a *Ce-rab7*-dependent manner. Such a requirement for rab7 activity in recycling from the early endosome could be specific for *C. elegans* or might have been missed using dominant negative techniques in mammalian cells, which presumably function by titrating out rab7 exchange factors rather than depleting the cell of rab7 itself (Feig, 1999). Alternatively, RME-2 might be recycled from late endosomes, as has been reported for LRP–receptor-associated protein complexes (Czekay *et al.*, 1997), in which case, *Ce-rab7*(RNAi) could inhibit RME-2 from reaching late endosomes for recycling. It will be interesting to differentiate between these models in future studies.

Much remains to be discovered about the mechanisms of endocytic trafficking. We anticipate that continued analysis of receptor-mediated endocytosis in the *C. elegans* oocyte, especially in-depth analysis of new *rme* mutants, identified in screens for defective yolk uptake, will contribute to our understanding of this important cellular process.

ACKNOWLEDGMENTS

We thank J. Fares, I. Greenwald, T. Schedl, H. Wilkinson, and Y. Zhang for helpful discussions during the course of this work; L. Pedraza for excellent technical assistance; T. Blumenthal, A. Fire, Y. Kohara, R. Plasterk, S. Strome, and H.G. van Luenen for reagents; and I. Greenwald, O. Hobert, H. Wilkinson, J. Yochem, T. Schedl, and Y. Zhang for comments on this manuscript. We thank Tim Schedl for unpublished information on the nature of ovulation defects in *rme-2* mutants. Many of the strains used in this work were

provided by the *Caenorhabditis* Genetics Center, which is funded by the National Center for Research Resources of the National Institutes of Health. This work was supported by National Institutes of Health National Service Research Award F32 GM19167-02 to B.G. and March of Dimes grant FY99-583 to D.H..

REFERENCES

Baker, M.E. (1988). Is vitellogenin an ancestor of apolipoprotein B-100 of human low-density lipoprotein and human lipoprotein lipase. Biochem. J. *255*, 1057–1060.

Bettinger, J.C., Lee, K., and Rougvie, A.E. (1996). Stage-specific accumulation of the terminal differentiation factor LIN-29 during *Caenorhabditis elegans* development. Development *122*, 2517–2527.

Bossinger, O., and Schierenberg, E. (1992). Cell-cell communication in the embryo of *Caenorhabditis elegans*. Dev. Biol. *151*, 401–409.

Bossinger, O., and Schierenberg, E. (1996). The use of fluorescent marker dyes for studying intercellular communication in nematode embryos. Int. J. Dev. Biol. *40*, 431–439.

Brenner, S. (1974). The genetics of *Caenorhabditis elegans*. Genetics *77*, 71–94.

Bucci, C. , Parton, R.G., Mather, I.H., Stunnenberg, H., Simons, K., Hoflack, B., and Zerial, M. (1992). The small GTPase rab5 functions as a regulatory factor in the early endocytic pathway. Cell *70*, 715–728.

Chalfie, M., Tu, Y., Euskirchen, G., Ward, W.W., and Prasher, D.C. (1994). Green fluorescent protein as a marker for gene expression. Science *263*, 802–804.

Chen, W.J., Goldstein, J.L., and Brown, M.S. (1990). NPXY, a sequence often found in cytoplasmic tails, is required for coated pit-mediated internalization of the low density lipoprotein receptor. J. Biol. Chem. *265*, 3116–3123.

Clandinin, T.R., DeModena, J.A., and Sternberg, P.W. (1998). Inositol trisphosphate mediates a RAS-independent response to LET-23 receptor tyrosine kinase activation in *C. elegans*. Cell *92*, 523–533.

Clark, S.G., Shurland, D.L., Meyerowitz, E.M., Bargmann, C.I., and van der Bliek, A.M. (1997). A dynamin GTPase mutation causes a rapid and reversible temperature-inducible locomotion defect in *C. elegans*. Proc. Natl. Acad. Sci. USA *94*, 10438–10443.

Czekay, R.P., Orlando, R.A., Woodward, L., Lundstrom, M., and Farquhar, M.G. (1997). Endocytic trafficking of megalin/RAP complexes: dissociation of the complexes in late endosomes. Mol. Biol. Cell *8*, 517–532.

Daro, E., Sheff, D., Gomez, M., Kreis, T., and Mellman, I. (1997). Inhibition of endosome function in CHO cells bearing a temperature-sensitive defect in the coatomer (COPI) component epsilon-COP. J. Cell Biol. *139*, 1747–1759.

de Camilli, P., Takei, K., and McPherson, P.S. (1995). The function of dynamin in endocytosis. Curr. Opin. Neurobiol. *5*, 559–565.

De Stasio, E., Lephoto, C., Azuma, L., Holst, C., Stanislaus, D., and Uttam, J. (1997). Characterization of revertants of unc-93(e1500) in *Caenorhabditis elegans* induced by *N*-ethyl-*N*-nitrosourea. Genetics *147*, 597–608.

Dell'Angelica, E.C., Shotelersuk, V., Aguilar, R.C., Gahl, W.A., and Bonifacino, J.S. (1999). Altered trafficking of lysosomal proteins in Hermansky-Pudlak syndrome due to mutations in the beta 3A subunit of the AP-3 adaptor. Mol. Cell *3*, 11–21.

Doniach, T., and Hodgkin, J. (1984). A sex determining gene, *fem-1*, required for both male and hermaphrodite development in *Caenorhabditis elegans*. Dev. Biol. *106*, 223–235.

Esser, V., Limbird, L.E., Brown, M.S., Goldstein, J.L., and Russell, D.W. (1988). Mutational analysis of the ligand binding domain of the low density lipoprotein receptor. J. Biol. Chem. *263*, 13282–13290.

Feig, L.A. (1999). Tools of the trade: use of dominant-inhibitory mutants of Ras-family GTPases. Nat. Cell Biol. *1*, E25–E27.

Feng, Y., Press, B., and Wandinger-Ness, A. (1995). Rab 7: an important regulator of late endocytic membrane traffic. J. Cell Biol. *131*, 1435–1452.

Ferguson, E.L., and Horvitz, H.R. (1985). Identification and characterization of 22 genes that affect the vulval cell lineages of the nematode *Caenorhabditis elegans*. Genetics *110*, 17–72.

Fire, A. (1986). Integrative transformation of *Caenorhabditis elegans*. EMBO J. *5*, 2673–2680.

Fire, A., Xu, S., Montgomery, M.K., Kostas, S.A., Driver, S.E., and Mello, C.C. (1998). Potent and specific genetic interference by double-stranded RNA in *Caenorhabditis elegans*. Nature *391*, 806–811.

Gafvels, M.E., Caird, M., Britt, D., Jackson, C.L., Patterson, D., and Strauss, J.F.d. (1993). Cloning of a cDNA encoding a putative human very low density lipoprotein/apolipoprotein E receptor and assignment of the gene to chromosome 9pter-p23. Somat. Cell Mol. Genet. *19*, 557–569.

Gaynor, E.C., Graham, T.R., and Emr, S.D. (1998). COPI in ER/Golgi and intraGolgi transport: do yeast COPI mutants point the way? Biochim. Biophys. Acta *1404*, 33–51.

Goldstein, J.L., Brown, M.S., Anderson, R.G., Russell, D.W., and Schneider, W.J. (1985). Receptor-mediated endocytosis: concepts emerging from the LDL receptor system. Annu. Rev. Cell Biol. *1*, 1–39.

Grant, B., and Greenwald, I. (1997). Structure, function, and expression of SEL-1, a negative regulator of LIN-12 and GLP-1 in *C. elegans*. Development *124*, 637–644.

Gu, J., Stephenson, C.G., and Iadarola, M.J. (1994). Recombinant proteins attached to a nickel-NTA column: use in affinity purification of antibodies. Biotechniques *17*, 257–262.

Hall, D.H., Winfrey, V.P., Blaeuer, G., Hoffman, L.H., Furuta, T., Rose, K.L., Hobert, O., and Greenstein, D. (1999). Ultrastructural features of the adult hermaphrodite gonad of *Caenorhabditis elegans*: relations between the germ line and soma. Dev. Biol. *212*, 101–123.

Herz, J., Hamann, U., Rogne, S., Myklebost, D., Gausepohl, H., and Stanley, K.K. (1988). Surface localization and high affinity for calcium for a 500-kd liver membrane protein closely related to the LDL-receptor suggest a physiological role as lipoprotein receptor. EMBO J. *7*, 4119–4127.

Horiuchi, H., *et al*. (1997). A novel rab5 GDP/GTP exchange factor complexed to rabaptin-5 links nucleotide exchange to effector recruitment and function. Cell *90*, 1149–1159.

Iwasaki, K., McCarter, J., Francis, R., and Schedl, T. (1996). *emo-1*, a *Caenorhabditis elegans* Sec61p gamma homologue, is required for oocyte development and ovulation. J. Cell Biol. *134*, 699–714.

Jones, A.R., Francis, R., and Schedl, T. (1996). GLD-1, a cytoplasmic protein essential for oocyte differentiation, shows stage- and sex-specific expression during *Caenorhabditis elegans* germline development. Dev. Biol. *180*, 165–183.

Jorgensen, E.M., Hartwieg, E., Schuske, K., Nonet, M.L., Jin, Y., and Horvitz, H.R. (1995). Defective recycling of synaptic vesicles in synaptotagmin mutants of *Caenorhabditis elegans*. Nature *378*, 196–199.

Kimble, J., and Sharrock, W.J. (1983). Tissue-specific synthesis of yolk proteins in *C. elegans*. Dev. Biol. *96*, 189–196.

Kramer, J.M., and Johnson, J.J. (1993). Analysis of mutations in the *sqt-1* and *rol-6* collagen gene of *Caenorhabditis elegans*. Genetics *135*, 1035–1045.

Lee, J., Jongeward, G.D., and Sternberg, P.W. (1994). *unc-101*, a gene required for many aspects of *Caenorhabditis elegans* development and behavior, encodes a clathrin-associated protein. Genes & Dev. *8*, 60–73.

Levy, A.D., Yang, J., and Kramer, J.M. (1993). Molecular genetic analysis of the *Caenorhabditis elegans dpy-2* and *dpy-10* collagen genes: a variety of molecular alterations affect organismal morphology. Mol. Biol. Cell *4*, 803–817.

Lowe, M., and Kreis, T.E. (1998). Regulation of membrane traffic in animal cells by COPI. Biochim. Biophys. Acta *1404*, 53–66.

McCarter, J., Bartlett, B., Dang, T., and Schedl, T. (1999). On the control of oocyte meiotic maturation and ovulation in *Caenorhabditis elegans*. Dev. Biol. *205*, 111–128.

McLauchlan, H., Newell, J., Morrice, N., Osborne, A., West, M., and Smythe, E. (1998). A novel role for Rab5-GDI in ligand sequestration into clathrin-coated pits. Curr. Biol. *8*, 34–45.

Mellman, I. (1996). Endocytosis and molecular sorting. Annu. Rev. Cell Dev. Biol. *12*, 575–625.

Mello, C.C., Kramer, J.M., Stinchcomb, D., and Ambros, V. (1991). Efficient gene transfer in *C. elegans*: extrachromosomal maintenance and integration of transforming sequences. EMBO J. *10*, 3959–3970.

Montgomery, M.K., Xu, S., and Fire, A. (1998). RNA as a target of double-stranded RNA-mediated genetic interference in *Caenorhabditis elegans*. Proc. Natl. Acad. Sci. USA *95*, 15502–15507.

Mukherjee, S., Ghosh, R.N., and Maxfield, F.R. (1997). Endocytosis. Physiol. Rev. *77*, 759–803.

Nonet, M.L., Grundahl, K., Meyer, B.J., and Rand, J.B. (1993). Synaptic function is impaired but not eliminated in *C. elegans* mutants lacking synaptotagmin. Cell *73*, 1291–1305.

Nigon, V. (1949). Les modalites de la reproduction et le determinisme du sexe chez quelques nematodes libres. Ann. Sci. Nat. *11*, 1–132.

Ohno, H., Aguilar, R.C., Yeh, D., Taura, D., Saito, T., and Bonifacino, J.S. (1998). The medium subunits of adaptor complexes recognize distinct but overlapping sets of tyrosine-based sorting signals. J. Biol. Chem. *273*, 25915–25921.

Ohno, H., Stewart, J., Fournier, M.C., Bosshart, H., Rhee, I., Miyatake, S., Saito, T., Gallusser, A., Kirchhausen, T., and Bonifacino, J.S. (1995). Interaction of tyrosine-based sorting signals with clathrin-associated proteins. Science *269*, 1872–1875.

Okkema, P.G., Harrison, S.W., Plunger, V., Aryana, A., and Fire, A. (1993). Sequence requirements for myosin gene-expression and regulation in *Caenorhabditis elegans*. Genetics *135*, 385–404.

Page, L.J., Darmon, A.J., Uellner, R., and Griffiths, G.M. (1998). L is for lytic granules: lysosomes that kill. Biochim. Biophys. Acta *1401*, 146–156.

Pearse, B.M., and Robinson, M.S. (1990). Clathrin, adaptors, and sorting. Annu. Rev. Cell Biol. *6*, 151–171.

Pfeffer, S.R. (1994). Rab GTPases: master regulators of membrane trafficking. Curr. Opin. Cell Biol. *6*, 522–526.

Press, B., Feng, Y., Hoflack, B., and Wandinger-Ness, A. (1998). Mutant Rab7 causes the accumulation of cathepsin D and cation-independent mannose 6-phosphate receptor in an early endocytic compartment. J. Cell Biol. *140*, 1075–1089.

Roth, T.F., and Porter, K.R. (1964). Yolk protein uptake in the oocyte of the mosquito *Aedes aegypti*. J. Cell Biol. *20*, 313–332.

Rothman, J.E., and Wieland, F.T. (1996). Protein sorting by transport vesicles. Science *272*, 227–234.

Sappington, T.W., and Raikhel, A.S. (1998). Molecular characteristics of insect vitellogenins and vitellogenin receptors. Insect Biochem. Mol. Biol. *28*, 277–300.

Sawamura, T., *et al*. (1997). An endothelial receptor for oxidized low-density lipoprotein. Nature *386*, 73–77.

Schekman, R., and Orci, L. (1996). Coat proteins and vesicle budding. Science *271*, 1526–1533.

Schneider, W.J. (1996). Vitellogenin receptors: oocyte-specific members of the low-density lipoprotein receptor supergene family. Int. Rev. Cytol. *166*, 103–137.

Schonbaum, C.P., Lee, S., and Mahowald, A.P. (1995). The *Drosophila* yolkless gene encodes a vitellogenin receptor belonging to the low density lipoprotein receptor superfamily. Proc. Natl. Acad. Sci. USA *92*, 1485–1489.

Sharrock, W.J. (1983). Yolk proteins of *C. elegans*. Dev. Biol. *96*, 182–188.

Sharrock, W.J., Sutherlin, M.E., Leske, K., Cheng, T.K., and Kim, T.Y. (1990). Two distinct yolk lipoprotein complexes from *Caenorhabditis elegans*. J. Biol. Chem. *265*, 14422–14431.

Shen, X., Steyrer, E., Retzek, H., Sanders, E.J., and Schneider, W.J. (1993). Chicken oocyte growth: receptor-mediated yolk deposition. Cell Tissue Res. *272*, 459–471.

Spieth, J., Nettleton, M., Zucker-Aprison, E., Lea, K., and Blumenthal, T. (1991). Vitellogenin motifs conserved in nematodes and vertebrates. J. Mol. Evol. *32*, 429–438.

Springer, T.A. (1998). An extracellular beta-propeller module predicted in lipoprotein and scavenger receptors, tyrosine kinases, epidermal growth factor precursor, and extracellular matrix components. J. Mol. Biol. *283*, 837–862.

Stifani, S., Barber, D.L., Nimpf, J., and Schneider, W.J. (1990). A single chicken oocyte plasma membrane protein mediates uptake of very low density lipoprotein and vitellogenin. Proc. Natl. Acad. Sci. USA *87*, 1955–1959.

Sudhof, T.C., Goldstein, J.L., Brown, M.S., and Russell, D.W. (1985). The LDL receptor gene: a mosaic of exons shared with different proteins. Science *228*, 815–822.

Ullrich, O., Reinsch, S., Urbe, S., Zerial, M., and Parton, R.G. (1996). Rab11 regulates recycling through the pericentriolar recycling endosome. J. Cell Biol. *135*, 913–924.

van der Sluijs, P., Hull, M., Webster, P., Male, P., Goud, B., and Mellman, I. (1992). The small GTP-binding protein rab4 controls an early sorting event on the endocytic pathway. Cell *70*, 729–740.

van Luenen, H.G.A.M., and Plasterk, R.H.A. (1997). Transposons. In: *C. elegans*, vol. II, ed. T. Blumenthal, D.L. Riddle, B.J. Meyer, and J.R. Priess, Cold Spring Harbor, NY: Cold Spring Harbor Laboratory Press, 97–116.

von Heijne, G. (1986). A new method for predicting signal sequence cleavage sites. Nucleic Acids Res. *14*, 4683–4690.

Wang, L.H., Sudhof, T.C., and Anderson, R.G. (1995). The appendage domain of alpha-adaptin is a high affinity binding site for dynamin. J. Biol. Chem. *270*, 10079–10083.

Wen, C., and Greenwald, I. (1999). p24 proteins and quality control of LIN-12 and GLP-1 trafficking in *Caenorhabditis elegans*. J. Cell Biol. *145*, 1165–1175.

Wendland, B., Emr, S.D., and Riezman, H. (1998). Protein traffic in the yeast endocytic and vacuolar protein sorting pathways. Curr. Opin. Cell Biol. *10*, 513–522.

Williams, B.D. (1995). Genetic mapping with polymorphic sequence-tagged sites. Methods Cell Biol. *48*, 81–96.

Yochem, J., and Greenwald, I. (1993). A gene for a low density lipoprotein receptor-related protein in the nematode *Caenorhabditis elegans*. Proc. Natl. Acad. Sci. USA *90*, 4572–4576.

Yochem, J., Tuck, S., Greenwald, I., and Han, M. (1999). A gp330/megalin-related protein is required in the major epidermis of *Caenorhabditis elegans* for completion of molting. Development *126*, 597–606.